Laser-Induced Decomposition and Ablation Dynamics Studied by Nanosecond Interferometry. 4. A Polyimide Film†

Tomokazu Masubuchi, Takuji Tada, Eiji Nomura, Koji Hatanaka,‡ Hiroshi Fukumura,‡ and Hiroshi Masuhara*

Department of Applied Physics, Osaka University, Suita, Osaka 565-0871, Japan

Received: July 3, 2001; In Final Form: January 16, 2002

Intense excimer laser excitation of polyimide film gives transient expansion and the following contraction, permanent swelling, and ablation, depending on excitation wavelength and fluence. Ablation by 248 nm excitation takes place only during the excitation laser pulse, and no debris were observed, while that by 351 nm excitation is brought about after sudden expansion. Permanent swelling was observed only for 351 nm excitation, and distinct differences in expansion and contraction behavior were observed between 248 and 351 nm excitation. On the basis of the morphological dynamics, it is shown that photochemical and photothermal mechanisms can explain mostly the results obtained by 248 and 351 nm excitation, respectively.

Introduction

Laser ablation of organic materials with intense ultraviolet excimer laser irradiation has received much attention as a potential technique to fabricate, modify, and functionalize material surface.[1−6] In addition to wide applications to various systems, it is worth noting that molecular processes during ablation constitute unique interesting physicochemical phenomena. Fundamental studies on the underlying mechanisms have been conducted mainly by using luminescence spectroscopy, transient absorption spectroscopy, photoaccoustic measurement, shadowgraphy, and so on.[7−15] It is indeed important to clarify nonlinear processes involving mutual interactions between excited states, cyclic multiphotonic absorption of excitation photons,[16,17] temperature elevation,[10,13,16] and ejection of fragmented products, leading to ablation. Recently, expansion and contraction of polymeric materials, which can be directly followed by measuring time-dependent surface displacement with nanosecond interferometry,[18−23] are pointed out to be essential to understanding ablation and related phenomena. Thus, photophysical and photochemical processes are now combined with surface morphological dynamics, opening a new research area of solid-state photochemistry.

In the case of poly(methyl methacrylate) (PMMA) film doped with biphenyl as a sensitizer, transient expansion started during the excitation laser pulse and then fragmented polymer debris were ejected explosively upon 248 nm excimer laser irradiation.[22] Below the threshold, expansion of the polymer film was also induced, but a flat surface was completely recovered via slow contraction. The morphological dynamics was considered in view of temperature elevation due to efficient photothermal conversion and glass−rubber transition of PMMA. Photochemical ablation was observed for triazenopolymer film, in which direct decomposition to gaseous products and surface movement dynamics due to its etching were directly measured in the time domain.[18] In the case of nitrocellulose/polyurethane film doped with a substituted copper phthalocyanine,[19] transient expansion and the following contraction were observed, while reduction of the thickness due to decomposition continues up to 1 μs. The behavior was well-explained in terms of endothermic degradation triggered by rapid photothermal conversion in the doped copper phthalocyanine.

Laser ablation of polyimide film has been studied extensively because polyimide is widely used as electronic device materials because of its excellent heat-resistant nature, insulation of electricity, and so on. Thus, elucidation of the underlying ablation mechanism of polyimide by utilizing nanosecond time-resolved interferometry is important and also useful for further application. Until now laser ablation of polyimide film has been considered on the basis of SEM observation,[24−26] time-of-flight[24] as well as conventional mass spectrometric analyses,[24] time-resolved photography,[27,28] AFM,[29,30] and so on at different excitation wavelengths. For example, it was reported that the ablation rate of polyimide film shows Arrhenius-type exponential dependence on laser fluence upon 248, 308, and 351 nm excitation, suggesting a photothermal ablation mechanism.[31] On the other hand, the etch rate obtained by 193 nm excitation is linear with the fluence, which was interpreted as a photochemical ablation mechanism.[32] It was also reported that main chains of polyimide were directly broken even by intense 248 and 308 nm excimer laser irradiation, demonstrating the importance of photochemical processes.[32] The ablation mechanism is furthermore discussed on the basis of recent experimental results.[33−35] Despite many investigations, the laser ablation mechanism of polyimide film has not been completely revealed yet.

In this article, we have applied nanosecond interferometry to polyimide film and studied its morphological changes upon intense KrF (248 nm) and XeF (351 nm) excimer laser irradiation. Depending on the laser fluence, polyimide film undergoes ablation, expansion, and contraction, and their combination constitutes very interesting photoinduced phenomena. On the basis of the morphological dynamics, we discuss underlying mechanisms of laser ablation and related behavior of polyimide film in detail.

† Part of the special issue "Noboru Mataga Festschrift".

* To whom correspondence should be addressed. E-mail: masuhara@ap.eng.osaka-u.ac.jp.

‡ Present address: Department of Chemistry, Tohoku University, Sendai, Miyagi 980-8578, Japan.

10.1021/jp012512l CCC: $22.00
Published on Web 02/05/2002

CHART I. Chemical Structure of the Used Polyimide

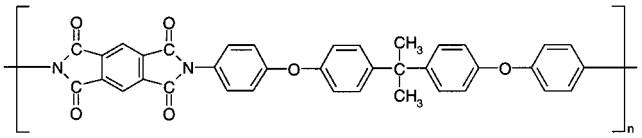

Experimental Section

Sample. A *N*-methyl-2-pyrrolidone solution of the precursor polymer (Nissan Chemical Ltd.) was spin-coated onto two kinds of quartz substrates and heated for 60 min at 250 °C to induce polymerization. The chemical structure of the prepared polyimide is given in Chart 1. The thickness of the film was ca. 1.5 μm, and the absorption coefficient of the film was 37.2 and 1.21 μm^{-1} at 248 nm and at 351 nm, respectively.

Ablation Experiment. A KrF excimer laser (Lambda Physik LEXTRA 200, 248 nm, 30 ns fwhm) or a XeF excimer laser (Lambda Physik LEXTRA 200, 351 nm, 30 ns fwhm) was used as an excitation pulse for inducing expansion/contraction, decomposition, swelling, and ablation. The fluence was adjusted with partially transmitting laser mirrors and was monitored shot-by-shot by a photodiode of which the output was corrected with a joulemeter (Gentec, ED-200) with an oscilloscope (Hewlett-Packard, HP54522A). A central area of the excimer laser pattern with a homogeneous intensity distribution was chosen with an appropriate aperture and then focused onto the sample surface by using a quartz lens ($f = 200$ mm). A fresh surface of the sample film was used in every measurement. Etch depth was measured by a surface depth profiler (Sloan, Dektak 3). All experiments were done in air at room temperature.

Nanosecond Time-Resolved Interferometry. The nanosecond time-resolved interferometry applied here is the same as reported before.[18−23] Briefly, the second harmonic pulse of a Q-switched Nd^{3+}:YAG laser (Continuum Surelite I, 532 nm, 10 ns fwhm) was used as a probe light for the Michelson-type interferometer to measure excimer laser-induced morphological changes of the present film. Interference patterns were acquired by a CCD camera. Time-resolved measurement was carried out by controlling the delay time (Δt) between excitation and probe laser pulses with a digital delay/pulse generator (Stanford Research System, DG 535). The delay time was monitored shot-by-shot by a digital oscilloscope. Here, we define $\Delta t = 0$ as the time when the peaks of both laser pulses coincide with each other. All data were obtained by one-shot measurement to avoid effects by exciting photoproducts formed by previous irradiation.

We have adopted two kinds of quartz substrate according to surface and internal configurations, as in the previous works.[18] In case of the surface configuration, fringe pattern results from an interference between the reference light from a standard reference mirror and the light reflected at the polymer surface. To avoid a disturbing interference due to a light reflected at the back surface of the quartz plate, a plate of which the two surfaces are not parallel with each other was used. Some representative interference patterns obtained with the surface configuration are given for laser-induced expansion below the ablation threshold and shown in Figure 1. In the experiment, a movement of the fringe to the left side represents an expansion of polymer film, which was confirmed by adjusting the optical condition. A shift of one fringe spacing to the left corresponds to an expansion of 266 nm, a half-wavelength of the probe laser. Deformation of the fringe pattern is clearly observed only in Figure 1b, which shows the transient morphological changes

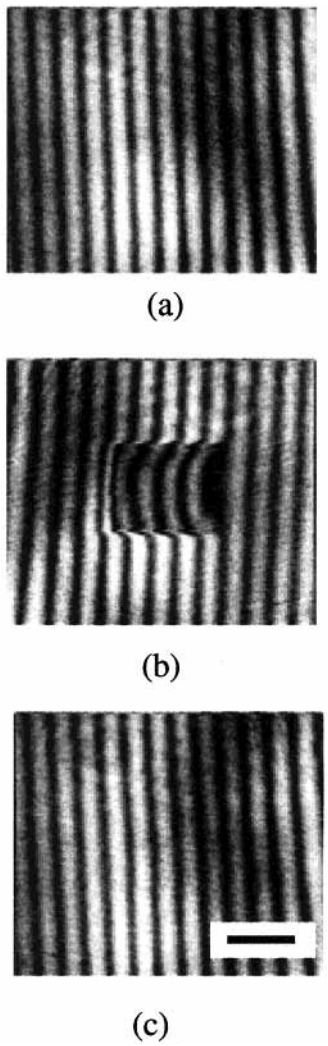

Figure 1. Nanosecond time-resolved interferometric images of polyimide film on a wedged quartz plate at the fluence of 130 mJ/cm^2 below the ablation threshold, which was obtained with the surface configuration (see text). The excitation wavelength is 351 nm. These images are all taken shot-by-shot at a fresh area of the same sample film. The fringe shift to the left represents an expansion. Delay times (Δt) are (a) $-\infty$ (before excitation), (b) 24 ns, and (c) ∞ (enough after excitation). The black bar in panel c indicates 1 mm in the image.

of the polyimide film below the ablation threshold. A shift by 0.8 of a fringe spacing to the left side is observed at the central part, giving an expansion of 210 nm. The shift of the fringe pattern decreased in a few tens of milliseconds, indicating contraction of the expanded film. Consequently, the initial flat surface was restored completely (Figure 1c).

Upon laser ablation, fragments or gaseous products are sometime ejected from the sample film and may vary the effective optical path length of the reflected light. The disturbance by the ejected products will lead to overestimation of the surface displacement of the irradiated polymer film. To overcome this problem, we use the internal configuration at which the surface of the quartz substrate, facing to the polymer film, and the back surface of the quartz plate are almost in parallel. The reflected light from the latter surface interferes with the reflected one from the polymer surface, generating interference fringe patterns. Because both reference and probe light beams are influenced similarly by fragments or products or both, refractive index change due to ejected fragments or gaseous products or both does not result in the shift of the interference patterns.

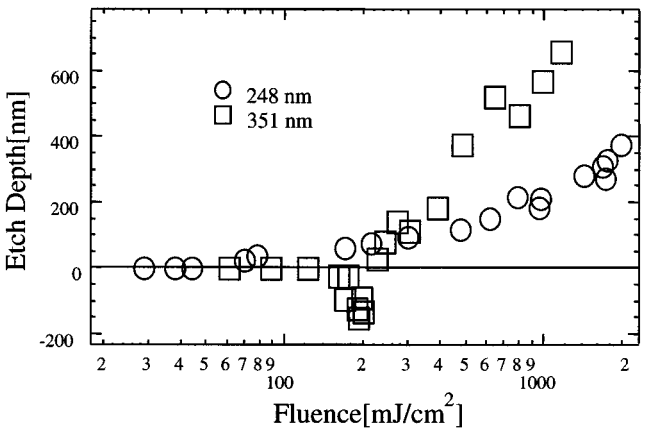

Figure 2. Etch depth profile of polyimide film obtained with 248 nm (○) and 351 nm (□) excimer laser irradiation.

Results and Discussion

Etch Depth. Fluence dependence of etch depth of the polyimide film is given in Figure 2, in which the ablation threshold was determined to be about 40 mJ/cm^2 and 210 mJ/cm^2 at 248 and 351 nm, respectively. At 248 nm excitation, the etch depth increases monotonically with the laser fluence. On the other hand, the film shows a permanent swelling (negative etching) from about 150 to 210 mJ/cm^2 at 351 nm excitation and undergoes laser ablation above the latter fluence. The interesting etching behavior, such as an enormous difference in the ablation threshold, depending on the excitation wavelength, may be ascribed to the absorption coefficient at the excitation wavelength. It is also expected that the ablation mechanism due to photochemical and photothermal degradation of the polymer depends on the energy of excitation photons. Here, we have conducted a series of the nanosecond time-resolved interferometric measurements for analyzing the morphological dynamics of polyimide leading to these permanent etchings and swellings.

Etching Dynamics Above the Ablation Threshold. Etching dynamics induced by 248 nm excimer laser irradiation above the ablation threshold is shown in Figures 3 and 4 in which the nanosecond time-resolved interferometric images are observed at the fluence of 550 and 210 mJ/cm^2, respectively. It is worth noting that expansion of the polyimide film was not observed clearly and etching started directly during the excimer laser pulse. Observation of etching behavior depends on the measurement optics of surface and internal configurations. The etching obtained with the surface configuration is always deeper than that with the internal configuration, which was already confirmed in laser ablation behavior of triazenopolymer film.[18] This difference is considered to be ascribed to the contribution of the effective refractive index change due to ejected products. It should be pointed out that interference patterns were always observed clearly in the irradiated area at all delay times. If products the size of which is comparable to the visible wavelength are ejected or the surface flatness is lost, interferometric images could not be observed or at least darkening should be detected. This is the case for laser ablation of a PMMA film doped with biphenyl or pyrene in which the explosive ejection

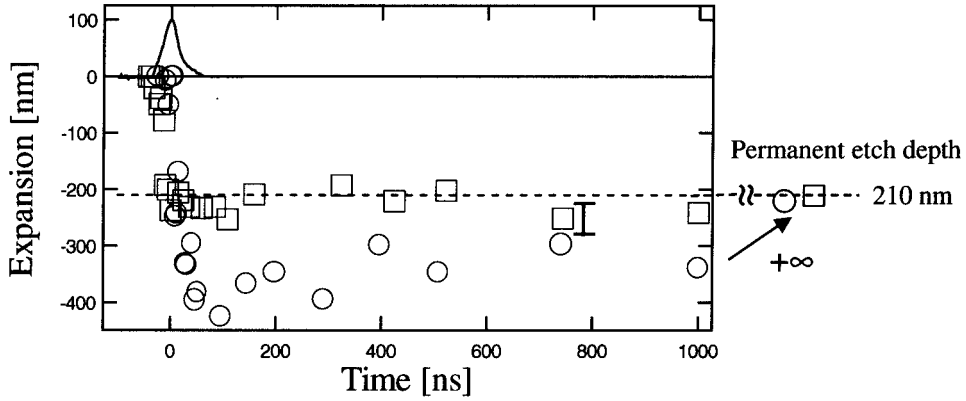

Figure 3. Expansion and etching dynamics of polyimide film at the fluence of 550 mJ/cm^2 above the ablation threshold with the surface configuration (○) and with the internal configuration (□). The dashed line represents the permanent etched depth (~210 nm), while the solid curve is an excimer laser pulse profile. The excitation wavelength is 248 nm.

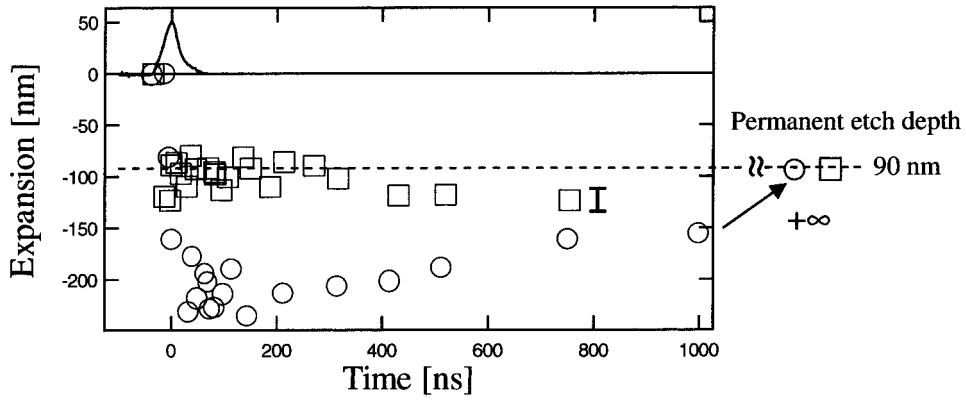

Figure 4. Expansion and etching dynamics of polyimide film at the fluence of 210 mJ/cm^2 above the ablation threshold with the surface configuration (○) and with the internal configuration (□). The dashed line represents the permanent etched depth (~90 nm), while the solid curve is an excimer laser pulse profile. The excitation wavelength is 248 nm.

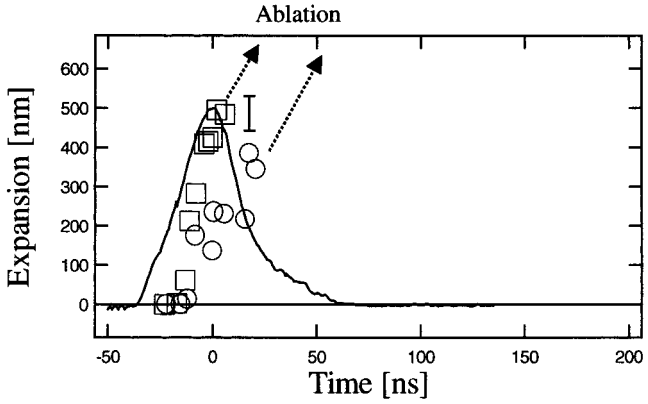

Figure 5. Expansion dynamics of polyimide film at the fluence of 460 (□) and 230 mJ/cm^2 (○) above the ablation threshold with the surface configuration. The solid curve represents an excimer laser pulse profile. The excitation wavelength is 351 nm. It becomes difficult to measure interferometric images after the time shown by arrows because of growing surface roughness and ejected debris.

of rather large fragmented debris led to shielding of the probe light.[9,22] The present results indicate that only gaseous products or at least small particles less than wavelength are generated and ejected by 248 nm laser irradiation. Also, it is deduced that the surface is always flat even during etching. The behavior is quite similar to laser ablation of triazenopolymer film.[18] It is also important to point out that the permanent etch depth of 210 and 90 nm at the fluence of 550 and 210 mJ/cm^2, respectively, is attained immediately, almost during the excimer laser pulse.

On the other hand, very rapid expansion was induced by the 351 nm excimer laser irradiation at the fluence of 460 and 230 mJ/cm^2 above the ablation threshold, as shown in Figure 5. The expansion started during the excimer laser pulse and reached several hundreds of a nanometer in a few tens nanoseconds. The starting time became earlier and the expansion speed was increased with the fluence. We could not observe any clear fringe pattern of interference images of the irradiated area at the stages later than 10 and 20 ns for the fluence of 460 and 230 mJ/cm^2, respectively. This is because the darkening of interference images was initiated. It is considered that the polymer surface became rough and fragmented debris were ejected.

Etching Mechanism. It is worth noting that ablation dynamics of polyimide film depends contrastively on excitation wavelength. The 248 and 351 nm excitation experiments give the dynamics similar to those of triazenopolymer[18] and of PMMA films,[22] respectively. Here, the interesting dependence is considered from two viewpoints. The first one is on the penetration depth of the excitation beam, which is determined by the absorption coefficient at the excitation wavelength. When the same number of photons are introduced to a sample film, the thickness of the excited surface layer is thinner for 248 nm than for 351 nm excitation. In other words, the excited state density is higher for 248 nm than for 351 nm. If bond cleavage of polyimide is induced similarly for both excitations, the chain length of the degradated polymer is longer for 351 nm than for 248 nm excitation. The higher excitation is necessary to bring about ablation for the 351 nm than for the 248 nm experiment, which is qualitatively consistent with the present etch depth measurements shown in Figure 2.

The second viewpoint is that the 248 nm photon has higher energy compared to 351 nm one. Photochemical reactions are probable for the 248 nm excitation, while photochemical decomposition is impossible for 351 nm excitation because all of the bond energies of C−C, C−N, and C−O are higher than that of the 351 nm photon. Absorbed energy should be eventually converted to heat, resulting in temperature elevation. This is a first approximation assuming that only linear absorption of excitation is realized. Successive two photon and cyclic multiphoton absorptions[17] should be involved to some extent, leading to photochemical decomposition. The density of decomposed sites is lower for this case compared with the 248 nm one-photon excitation so that the degraded polymer should be longer.

The present interferometric studies can be interpreted well by considering that, upon 248 nm excitation, main chains of polyimide could be broken densely and small decomposed products were formed. As the etching proceeds during the excitation pulse as shown in Figures 3 and 4, the decomposition may start almost instantaneously and be completed soon. As a result rather longer polymer chains, which are necessary for expansion, were not left appreciably. On the other hand, main chains cannot be decomposed efficiently to low molecular weight polymers by 351 nm one-photon excitation, and photothermal temperature elevation and two-photon photochemical decomposition mentioned above are considered to have important roles in ablation. The photothermal nature in 351 nm etching is in good agreement with the recent results by Ortelli et al.[36,37] Consequently, the fragmented debris were formed, and their explosive ejection was initiated. The size of debris may be larger than or comparable to the observation wavelength and/or the surface may be left rough, leading to the darkening. Thus, etching/ablation dynamics above the ablation threshold are different between 248 and 351 nm. It is generally considered that extra energy in photochemical decomposition and heat generated by recombination of decomposed molecules results in rapid temperature elevation, assisting thermal degradation further, so that both decomposition mechanisms are in principle closely coupled with each other. It is critical to determine the relative contribution of photochemical and photothermal ablation mechanisms upon the laser ablation; however, a photochemical ablation mechanism of polyimide film at 248 nm is proposed here in view of the present interferometry measurement. This explanation on mechanism is well-supported by analyzing laser-induced dynamics below the ablation threshold, which is described in the following sections.

Expansion/Contraction Dynamics Below the Ablation Threshold. At 248 nm excitation, expansion and contraction dynamics is given in Figure 6 at the fluence of 20 mJ/cm^2. The irradiated film began to expand during the excimer laser pulse and contracted rapidly. The rate of expansion and contraction is about 1 and 0.1 nm/ns, respectively. The maximum expansion amplitude was attained when the excitation pulse ends, and the expansion disappeared completely after a few milliseconds. It is notable that the original flat surface was recovered well and the clear fringe pattern was observed at any delay time.

Expansion dynamics at 351 nm excitation with the fluence of 80 and 130 mJ/cm^2 below the ablation threshold is shown in Figure 7. The irradiated film began to expand during the excimer laser pulse similarly as that at 248 nm excitation, and the expansion amplitude increased with the fluence. The expansion was reduced quite slowly, except a small hump at 130 mJ/cm^2, and then the original flat surface was recovered.

First, we consider that the different expansion behavior at 248 and 351 nm excitation is due to the different etchingmechanism discussed above. In the case of 351 nm excitation,

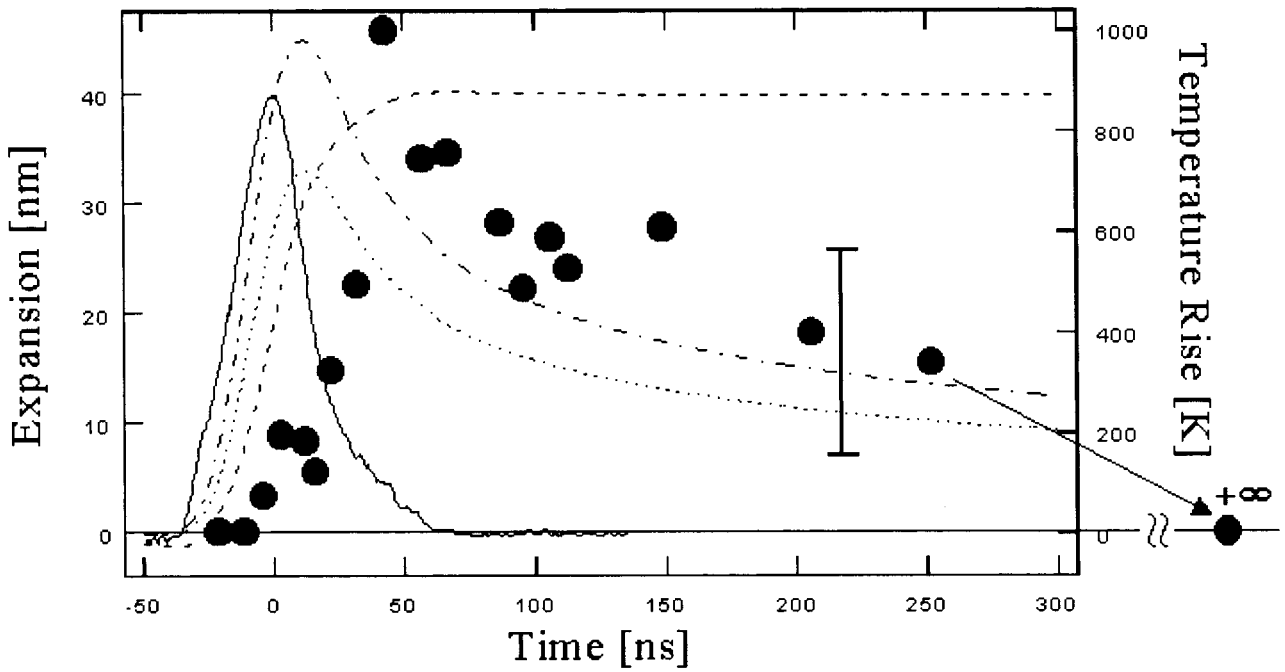

Figure 6. Expansion and contraction dynamics of polyimide film at the fluence of 20 mJ/cm^2 below the ablation threshold with the surface configuration. The solid and dash−dotted curves represent the time profiles of the excimer laser pulse and time-integration of the laser pulse, respectively, while the dotted and dash−dotted curves are simulated surface temperature rise at the fluence of 20 and 30 mJ/cm^2, respectively. The excitation wavelength is 248 nm.

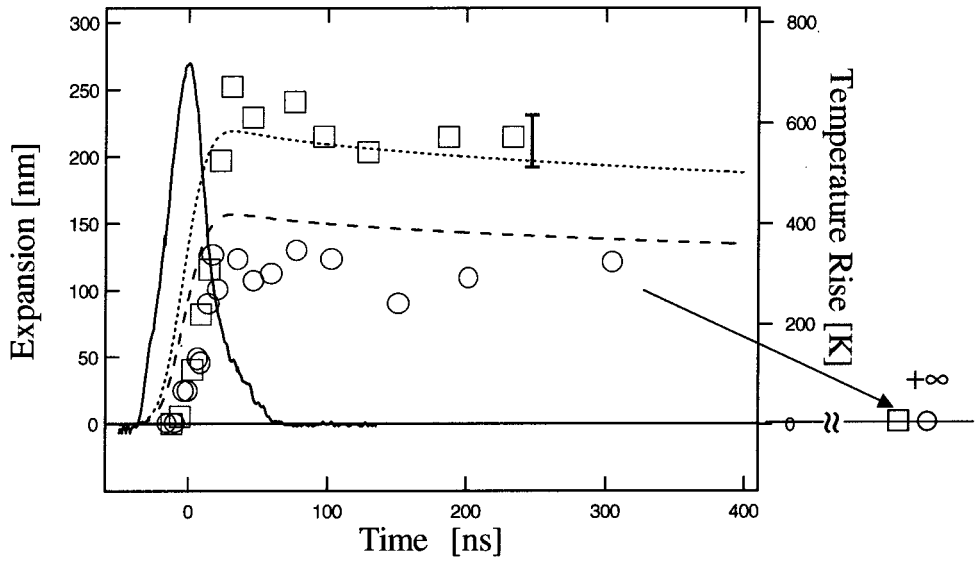

Figure 7. Expansion and contraction dynamics of polyimide film at the fluence of 80 (○) and 130 mJ/cm^2 (□) below the ablation threshold with the surface configuration. The solid curve represents the time profile of the excimer laser pulse. The dotted and dashed curves represent the simulated surface temperature rise at the fluence of 80 and 130 mJ/cm^2, respectively. The excitation wavelength is 351 nm.

multiphoton photochemical and photothermal processes are involved and the latter may be more important at lower fluence. The contraction behavior at 80 mJ/cm^2 may reflect slow heat dissipation in the polyimide, which behavior is actually consistent with the photothermal expansion and contraction dynamics of a PMMA film.[20] On the other hand, the thin surface layer is excited at 248 nm so that heat dissipation to the quartz substrate should be slower than that at 351 nm. To understand the expansion and contraction dynamics, a more quantitative analysis of cooling processes by the following simulation seems hopeful.

Simulation of Surface Temperature. Here, we assume a photothermal mechanism even for 248 nm excitation and estimate the temperature rise and decay dynamics. Because high-intensity excitation is confined at the thin surface layers of 27 and 830 nm thickness for 248 and 351 nm excitation, respectively, assuming that the Lambert−Beer law holds, temperature elevation is extremely large. Here, the surface of the 20 nm thickness is numerically examined for both excitation wavelengths. We have calculated surface temperature rise as a function of delay time by solving the one-dimensional heat conduction equation. In the calculation, we assumed that the absorption coefficient of α, heat conductance, and density are independent upon both temperature and excitation intensity, the Lambert−Beer law holds, and the absorbed photon energy is fully converted to heat. We used a heat conductance[38] of 1.20×10^{-3} W/(cm K), a density[39] of 1.42 g/cm^3 for polyimide, and the following temperature-dependent specific heat:[31]

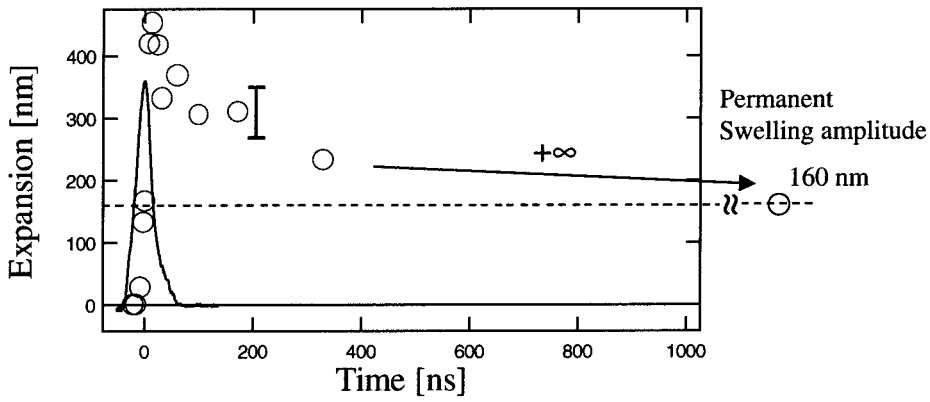

Figure 8. Expansion and contraction dynamics of polyimide film at the fluence of 170 mJ/cm^2 near the ablation threshold with the surface configuration. The dashed line represents the permanent swelling amplitude (~160 nm), while the solid curve represents an excimer laser pulse profile. The excitation wavelength is 351 nm. The arrow shows the time range during which the fringe pattern could not be observed.

$$C_P(T) = 0.96 + 1.39((T - 300)/400) - 0.43((T - 300)/400)^2$$

where T is temperature.

The calculated surface temperature rise for each excitation condition is given in Figures 6 and 7. Upon 248 nm excitation, the surface temperature reaches 1010 and 1280 K at the fluence of 20 and 30 mJ/cm^2, respectively. On the other hand, the degradation temperature of polyimide is experimentally determined to be about 700 K.[40] It is noticeable that the calculated temperature is higher than 700 K but attained only for a few hundred nanoseconds. This suggests that photothermal degradation is not probable, because polyimide degradation at 700 K was confirmed by 100 min heating. In the case of 351 nm excitation, the estimated peak temperature is 690−860 K at the fluence of 80−130 mJ/cm^2. Because temperature decreases by 100 K take only 400 ns, thermal degradation again seems impossible. The expansion and contraction dynamics is qualitatively consistent with the simulated temperature change, particularly at 80 mJ/cm^2. This is quite reasonable because the expansion amplitude should be proportional to the temperature elevation. Thus, morphological dynamics obtained at 351 nm excitation can be interpreted in terms of photothermal processes described above.

On the other hand, the rapid decay component observed at 248 nm excitation, was not reproduced by this simulation. Namely, photochemical decomposition, which is now not induced densely at 20 mJ/cm^2, may result in gaseous small molecules, and their leakage to air or recombination are probably responsible for the behavior. This explanation is consistent with the behavior just below the threshold.

Expansion/Contraction Dynamics and Permanent Swelling Just Below the Ablation Threshold. Expansion and contraction dynamics at 351 nm excitation with the fluence of 170 mJ/cm^2, a little below the ablation threshold, was given in Figure 8. Transient expansion started during the excimer laser pulse similarly as above the ablation threshold, and its expansion rate is extremely large at a few tens nanometers per nanosecond. On the other hand, contraction speed in a few hundred nanoseconds range is estimated to be about 1 nm/ns, and later, the contraction becomes slow, and the original surface was not recovered. Though the fringe patterns in interference images of the area irradiated by the excimer laser were measured at the earlier stages and enough after excitation (permanent swelling), we could not observe them at the stages later than 330 ns, which is due to the darkening. This means that the film surface lost enough flatness in a few hundred nanoseconds. The shrinking with time may recover surface roughness less than wavelength order.

It should be noticed that the rapid decay in Figure 8 is similar to that at 248 nm excitation in Figure 6. The excitation may be high enough to induce two-photon and cyclic multiphoton absorptions, leading to photodecomposition. The produced small molecules undergo leakage to the air or recombination, giving the rapid contraction. This is consistent with the explanation given above.

Summary

On the basis of the results above and below the ablation threshold, we can discuss the underlying mechanism giving the present etching, expansion, and contraction. At high fluence above the ablation threshold, etching dynamics at 248 and 351 nm can be ascribed mainly to photochemical and photothermal processes, respectively. At 351 nm excitation, expansion and contraction dynamics at low fluence is consistent with the simulation of temperature rise. This means that photothermal mechanism surely holds for this case. Just below the threshold, a hump in the expansion and contraction profile becomes clear, indicating an additional process is involved. In the case of 248 nm excitation, this hump is also observed clearly even at very low fluence. Thus, we consider that the hump is not due to a photothermal origin. Because the 248 nm etching is regarded as photochemical process, we consider that the rapid expansion and fast contraction with in 1 nm/ns is due to photochemical formation and recombination/leakage of decomposed small molecules. The decomposition will be realized not only by 248 nm one-photon excitation but also by 351 nm two-photon and cyclic multiphoton excitation. However, the 351 nm etching has a strong photothermal nature, which is reasonable because two-photon excitation is still not major in the nanosecond irradiation experiment.

Acknowledgment. The present work is partly defrayed by the Grant-in-Aid for Scientific Research on Priority Area (B) on "Laser Chemistry of Single Nanometer Organic Particles" from the Ministry of Education, Science, Sports, and Culture of Japan (Grant 10207204). Thanks are also due to reviewers for their kind comments and discussion.

References and Notes

(1) Srinivasan, R.; Mayne-Banton, V. *Appl. Phys. Lett.* **1982**, *41*, 576.
(2) Andrew, J. E.; Dyer, P. E.; Forster, D.; Key, P. H. *Appl. Phys. Lett.* **1988**, *52*, 1880.
(3) Masuhara, H.; Hiraoka, H.; Domen, K. *Macromolecules* **1987**, *20*, 450.

(4) Niino, H.; Nakano, M.; Nagano, S.; Yabe, A.; Miki, T. *Appl. Phys. Lett.* **1989**, *55*, 510.
(5) Dyer, P. E.; Farley, R. *Appl. Phys. Lett.* **1990**, *57*, 765.
(6) Lippert, T.; Gerber, T.; Wokaun, A.; Funk, D. J.; Fukumura, H.; Goto, M. *Appl. Phys. Lett.* **1999**, *75*, 1018.
(7) Tsuboi, Y.; Hatanaka, K.; Fukumura, H.; Masuhara, H. *J. Phys. Chem.* **1994**, *98*, 11237.
(8) Tsuboi, Y.; Fukumura, H.; Masuhara, H. *J. Phys. Chem.* **1995**, *99*, 10305.
(9) Fukumura, H.; Takahashi, E.; Masuhara, H. *J. Phys. Chem.* **1995**, *99*, 750.
(10) Fujiwara, H.; Fukumura, H.; Masuhara, H. *J. Phys. Chem.* **1995**, *99*, 11844.
(11) Hatanaka, K.; Kawao, M.; Tsuboi, Y.; Fukumura, H.; Masuhara, H. *J. Appl. Phys.* **1997**, *82*, 5799.
(12) Tsuboi, Y.; Hatanaka, K.; Fukumura, H.; Masuhara, H. *J. Phys. Chem. A* **1998**, *102*, 1661.
(13) Fujiwara, H.; Nakajima, Y.; Fukumura, H.; Masuhara, H. *J. Phys. Chem.* **1995**, *99*, 11481.
(14) Bennett, L. S.; Lippert, T.; Furutani, H.; Fukumura, H.; Masuhara, H. *Appl. Phys. A* **1996**, *63*, 327.
(15) Tsuboi, Y.; Fukumura, H.; Masuhara, H. *Appl. Phys. Lett.* **1994**, *64*, 2745.
(16) Fukumura, H.; Mibuka, N.; Eura, S.; Masuhara, H.; Nishi, N. *J. Phys. Chem.* **1993**, *97*, 13761.
(17) Fukumura, H.; Masuhara, H. *Chem. Phys. Lett.* **1994**, *221*, 373.
(18) Furutani, H.; Fukumura, H.; Masuhara, H.; Lippert, T.; Yabe, A. *J. Phys. Chem. A* **1997**, *101*, 5742.
(19) Furutani, H.; Fukumura, H.; Masuhara, H.; Kambara, S.; Kitaguchi, T.; Tsukada, H.; Ozawa, T. *J. Phys. Chem. B* **1998**, *102*, 3395.
(20) Furutani, H.; Fukumura, H.; Masuhara, H. *J. Phys. Chem.* **1996**, *100*, 6871.
(21) Furutani, H. Ph. D Thesis (in Japanese), Osaka University, Suita, Osaka, Japan, 1996.
(22) Furutani, H.; Fukumura, H.; Masuhara, H. *Appl. Phys. Lett.* **1994**, *65*, 3413.
(23) Masuhara, H.; Sasaki, K.; Fukumura, H.; Furutani, H. *Analyst* **1998**, *123*, 531.
(24) Krajnovich, D. J. *J. Appl. Phys.* **1997**, *82*, 427.
(25) Hahn, D. W.; Ediger, M. N.; Pettit, G. H. *J. Appl. Phys.* **1995**, *77*, 2759.
(26) Koren, G.; Yeh, J. T. C. *J. Appl. Phys.* **1984**, *56*, 2120.
(27) Dyer, P. E.; Sidhu, J. *J. Appl. Phys.* **1988**, *64*, 4657.
(28) Srinivasan, R.; Casey, K. G.; Braren, B.; Yeh, M. *J. Appl. Phys.* **1990**, *67*, 1604.
(29) Cooper, J. B.; Julian, B.; Morrison, H.; Song, P.; Albin, S.; Zheng, J. *Thin Solid Films* **1997**, *303*, 180.
(30) Piglmayer, K.; Arenholz, E.; Ortwein, C.; Arnold, N.; Bäuerle, D. *Appl. Phys. Lett.* **1998**, *73*, 847.
(31) Kuper, S.; Brannon, J.; Brannon, K. *Appl. Phys. A* **1993**, *56*, 43.
(32) Srinivasan, R.; Braren, B.; Dreyfus, R. W. *J. Appl. Phys.* **1987**, *61*, 372.
(33) Arnold, N.; Bityurin, N. *Appl. Phys. A* **1999**, *68*, 615.
(34) Luk'yanchuk, B.; Bityurin, N.; Himmelbauer, M.; Arnold, N. *Nucl. Instrum. Methods Phys. Res., Sect. B* **1997**, *122*, 347.
(35) Schmidt, H.; Ihlemann, J.; Wolff-Rottke, B.; Luther, K.; Troe, J. *J. Appl. Phys.* **1998**, *83*, 5458.
(36) Ortelli, E. E.; Geiger, F.; Lippert, T.; Wei, J.; Wokaun, A. *Macromolecules* **2000**, *33*, 5090.
(37) Ortelli, E. E.; Geiger, F.; Lippert, T.; Wokaun, A. *Appl. Spectrosc.* **2001**, *55*, 412.
(38) Feurer, T.; Wahl, S.; Langhoff, H. *J. Appl. Phys.* **1993**, *74*, 3523.
(39) Brunco, D. P.; Thompson, M. O.; Otis, C. E.; Goodwin, P. M. *J. Appl. Phys.* **1992**, *72*, 4344.
(40) Numata, S.; Kinjo, N. *Kobunshi Ronbunshu* **1985**, *42*, 7.